A New Scanning Approach for Limb Extremities using a Water Bag in Freehand 3D Ultrasound

Q.H. Huang and Y.P. Zheng

Rehabilitation Engineering Center, The Hong Kong Polytechnic University, Kowloon, Hong Kong SAR, China

Running Title: 3D Ultrasound using Water Bag

Corresponding author:

Yongping Zheng, PhD.

Rehabilitation Engineering Center,

The Hong Kong Polytechnic University,

Hung Hom, Kowloon, Hong Kong SAR, P.R.China

Tel: 852-27667664

Fax: 852-23624365

Email: ypzheng@ieee.org

ABSTRACT

3D ultrasound can significantly improve the visualization of musculoskeletal tissues, such as residual limbs, feet and hands. Traditionally, mechanical scanning is normally required to obtain the entire volume of these limb extremities. In this paper, a new scanning approach using a water bag was described to collect the complete volume of various tissues surrounding bones. The water bag was used to contain the limb extremity and the scanning was conducted on its external surface from different directions. The recorded 2D ultrasound images containing complete anatomic information surrounding the bones from different directions were used to form full 3D volumes of the limb extremities. A plastic auxiliary apparatus was designed to hold the water bag and support the subject's limb part with an armrest. A corresponding algorithm was proposed to remove invalid image information within each sweep by a separating plane defined semiautomatically. Two phantoms were used to test the repeatability and accuracy of the imaging. The distance between two plastic bands attached to a plastic tube filled with ultrasound gel measured by a micrometer and from the four reconstructed volumes were 39.03±0.36 mm and 39.2±0.5 mm, respectively. The diameter, height and volume of a silicone cylinder phantom measured for the 10 reconstructed volumes were 40.2±1.4 mm, 12.9±1.0 mm and 16400±1600 mm^3, respectively. They agreed with the corresponding results obtained by the micrometer, which were 41.29±0.13 mm, 12.98±0.17 mm and 17370±140 mm^3, respectively. The reconstructed volumes of the two phantoms, a chicken leg *in vitro*, and human fingers *in vivo* were also reported. The preliminary results obtained in this study demonstrated that this new scanning approach

should have potential for the 3D ultrasound imaging of musculoskeletal extremities using freehand scanning. (E-mail: ypzheng@ieee.org)

Keywords: Three-dimensional ultrasound, 3D ultrasound, musculoskeletal tissues, limb extremity, water bag.

Introduction

Growing attention has been paid to musculoskeletal tissues using high resolution ultrasound in recent years (Winter et al. 2001; Martinoli et al. 2002). Despite of many successful examinations, one of the limitations of 2D sonography is that the clinician cannot build up an accurate 3D structure of anatomy based on multiple 2D B-mode images; hence, the measurements in 3D space are unavailable. 3D ultrasound has proven to be a powerful tool, which is capable of overcoming this problem by reconstructing 3D volumes (Nelson and Pretorius 1998). Moreover, freehand 3D ultrasound has demonstrated its advantages in the applications of musculoskeletal tissues with the lower cost and the more convenient operation in comparison with other types of 3D ultrasound acquisition protocols (Gee et al. 2003a; Treece et al. 2002; Huang et al. 2005).

Figure 1 shows the diagram of a typical freehand 3D ultrasound imaging system, where the ultrasound probe with an attached electromagnetic spatial sensor is held by the operator's hand and moved over the surface of tissue. The sequential B-mode images, with corresponding position and orientation information sensed by the spatial sensor, are produced by the system and then transferred to a computer with the software programmed for data acquisition, signal processing, volume reconstruction and

subsequent analysis. In order to obtain accurate locations of 3D anatomy, the subject's body part should be kept as still as possible during the data acquisition. The currently used scanning methods require the body part to be maintained in steady state on a fixed plate. The scanning process can be performed by guiding the ultrasound probe over the exposed surface of the body part. However, for musculoskeletal body parts, only the soft tissues between the ultrasound probe and the underlying bones can be correctly imaged because of a strong attenuation of ultrasound beam by the overlying bones and soft tissues. The image information of the tissue at the location deeper than the bone interface on the collected 2D ultrasound images are not real but consists of artifacts caused by the attenuation and will affect the quality of 3D reconstruction (Fig. 2). As a result, based on the current scanning methods, only one side of a musculoskeletal body part can be correctly imaged and reconstructed in 3D.

Although the reconstructed volume containing incomplete anatomical structure based on freehand 3D ultrasound can suffice in many clinical applications, it is very important to construct a volume with complete 3D anatomy information surrounding the bones, especially for limb extremities in many areas, such as the prosthetic socket design for residual limbs (Douglas et al. 2002) and musculoskeletal modeling (Lieber and Friden 2000). One possible solution to achieve complete scanning is to scan around the limb extremity covered by ultrasound gel. Since there is a direct contact between the probe and the limb surface, the soft tissues will be deformed to cause error (Gee et al. 2003b; Treece et al. 2002). The compression will also affect the positioning of the limb extremity, i.e., it keeps moving during the scanning. In addition, scanning body parts with irregular shapes, such as hands and fingers, will be very difficult using this approach, as the ultrasound gel

may not be able to fill all the gaps between the probe and the tissue and between the body parts. Submerging the probe and the operator's hand into a big water tank is another potential solution, but it may not be convenient in many cases. He et al. (1996) developed a mechanical localizer to conduct rotary scanning around the residual limb immersed in a water tank. Image compounding was also applied to the overlapped region of those B-mode images locating in same plane. The final compounded images in different planes could be reconstructed as a 3D volume. However, no study has been previously reported on using tracked freehand techniques for collecting 3D volumes of limb parts with complete anatomic structures.

In this study, we investigated the limitations of the conventional scanning approach for freehand 3D ultrasound and designed a new scanning protocol using a water bag. This new approach could allow the operator globally to scan the limb extremity submerged in the water bag from different directions and reconstruct a complete volume of the limb anatomy surrounding bones. Multiple freehand sweeps (Gee et al. 2003b), each of which had unique probing direction and moving direction, were implemented to cover the entire anatomy of interest. Moreover, as the ultrasound probe was moved along the external surface of the water bag, the tissue deformation caused by the direct contact between the ultrasound probe and the subject's skin surface could be avoided. To improve the quality of 3D volumes, a new method was proposed rapidly to separate the invalid image contents caused by ultrasound attenuation from the valid data within a sweep by semiautomatically defining a separating plane. The volume reconstruction could only make use of those pixels within the valid region. In the following sections, the

novel scanning protocol using a water bag is described in detail, together with preliminary results of two phantoms, animal tissues *in vitro* and human tissues *in vivo*.

Methods

System overview

A corresponding freehand 3D ultrasound imaging system was developed and successfully used for musculoskeletal tissues (Huang et al. 2005). As illustrated in Fig. 1, this portable system was comprised of three main components:

- A portable medical ultrasound scanner with a linear probe at 7.5 MHz (SonoSite 180PLUS, SonoSite, Inc., Bothell, WA, USA).
- An electromagnetic spatial sensing device (MiniBird Manual, Ascension Technology Corporation, Burlington, VT, USA) for recording the position and orientation of the probe in real time.
- A PC (2.4 GHz Pentium IV microprocessor and 512 M bytes RAM) installed with a digital video capture card (NI-IMAQ PCI/PXI-1411, National Instruments Corporation, Austin, TX, USA) and a custom-designed program for data acquisition, processing, volume reconstruction and analyses.

During an examination, a sequence of ultrasound B-mode images corresponding to the cross-sections of the body part was produced by the ultrasound scanner. Meanwhile, the spatial information, including three positions (t_x, t_y, t_z) and three angles (azimuth, elevation, roll), were sensed by the spatial sensor attached to the linear ultrasound probe and then transferred from the control box of the spatial sensing device to the computer through a RS232 serial port. The captured B-mode images were digitized by the video

capture card and recorded with corresponding 3D spatial information. The acquired data were processed and analyzed by the program for visualization and reconstruction.

Temporal and spatial calibration experiments were performed for the system. Based on a previously reported method (Treece et al. 2003), we developed an improved method using a 3D translating device (Parker Hannifin Corporation, Irvine, CA, USA) to control the movement of the ultrasound probe during the temporal calibration. The ultrasound probe was immersed in a tank filled with water and moved up and down by the 3D translating device. The normalized positions of the lines denoting the bottom of the water tank in B-scan images were correlated with those measured by the spatial sensor. The optimum time delay between the captured images and sensed spatial data could be obtained by finding out the minimum RMS difference between the two data streams. After that, the spatial calibration was performed using a cross-wire phantom (Barry et al. 1997). Two cotton wires were crossed in a water tank. In each experiment, around 60 B-scans, as well as corresponding spatial information, were recorded from various directions. The positions of the crosses in each B-scan were manually marked and then calculated using a Levenberg-Marquardt nonlinear algorithm to achieve spatial relationship between the image plane and the spatial sensor (Prager et al. 1998). In our previous report (Huang et al. 2005), three validation phantoms with regular shapes were used quantitatively to assess the accuracy of the system. The average errors in three orthogonal directions were 0.1±0.4 mm, -0.3±0.3 mm and 0.3±0.4 mm, respectively.

Scanning protocol

To achieve our purpose of constructing a 3D volume containing complete anatomic information, water bags with different sizes and shapes were designed for various kinds of limb extremities, such as hands, feet and residual limbs. A plastic auxiliary apparatus (Fig. 3) was also designed to fix the water bag and support the limb part to be scanned. To obtain ultrasound images without significant attenuation, the wall of the water bag was thin enough to allow the ultrasound signals to propagate through. During the scanning process, the limb extremity was immersed in the bag filled with water and the probe was manually held and moved on the external surface of the water bag. Ultrasound gel was applied on the surface of the water bag before scanning. Figure 4 illustrates this scanning protocol using the water bag.

Although the new scanning protocol could achieve global information of 3D anatomy, the speckles behind the bones in the captured 2D images introduced a great source of error into the reconstructed volume. Due to the large attenuation caused by the strong reflection on the bone surface and the strong scattering inside the bone, there should have no ultrasound signals behind the bones. However, due to multiple reflections and other artifacts, speckles normally exist behind the bone and they may affect the quality of the volume reconstruction. Manually removing these speckles frame-by-frame would take too much time and was not practicable for clinical applications. In addition, there is lack of robust algorithms for automatically identifying these speckles in B-mode images, due to the complexity of musculoskeletal tissues. To solve this problem, the scanning process in this study was regulated by using multiple sweeps, each of which had unique probing direction and moving direction (Fig. 5a). Provided that the limb extremity

being scanned was kept steady enough, the global scanning could be realized by taking multisweep freehand acquisition to cover the entire limb extremity from different directions (Fig. 5b). Consequently, the 3D volume could be reconstructed by combining multiple sweeps into a single 3D cuboid with respect to their relative spatial locations, as illustrated in Fig. 5c.

Semiautomatic removal of unnecessary speckles behind the bone

As discussed above, most unnecessary speckles in a B-mode image usually appear below the bones. Within a single sweep, if the 3D location of a bone can be obtained, the lower region showing the unnecessary speckles in the captured images can be located and discarded. In this study, a semiautomatic method was proposed to find a separating plane (Fig. 6), by which the region to be retained could be separated from that to be discarded. However, a separating plane in a sweep could not completely extract the unnecessary speckles, if the structures of bones were too complex. In this study, a single sweep was required to contain the bones with relatively uniform shapes and approximately linear along the scanning directions so that the separating plane was able to be applied for the segmentation. Fortunately, most of human limb extremities conform to this requirement. If the structure of the limb extremity to be scanned was curved, the single sweep on one side could be divided into several subsweeps, within each of which the bone structure appeared to be approximately linear. Therefore, the separating planes for the subsweeps could be respectively defined.

As shown in Fig. 7a, two lines ($\overline{AB}$, $\overline{CD}$) for separating the valid and the invalid region in ultrasound images were manually marked in two arbitrary B-mode images,

respectively, where the bones could be obviously observed. With respect to the two origin points and two distal points (*A*, *B*, *C*, *D*) denoting the two selected separating lines, a center point *O* and four corresponding vectors were defined as follow:

$$O = \left(A + B + C + D\right)/4, \tag{1-1}$$

$$V_{AB} = B - A, \tag{1-2}$$

$$V_{CD} = D - C, \tag{1-3}$$

$$V_{AC} = C - A, \tag{1-4}$$

$$V_{BD} = D - B. \tag{1-5}$$

As shown in Fig. 7b, the four vectors could be used to calculate two averaged vectors as follows:

$$V_1 = \frac{\left(V_{AB} + V_{CD}\right)}{2}, \tag{2-1}$$

$$V_2 = \frac{\left(V_{AC} + V_{BD}\right)}{2}. \tag{2-2}$$

In this study, the cross-product ($\hat{N}$) of the two normalized vectors ($\hat{V}_1$, $\hat{V}_2$) was recognized as the normal of the separating plane (Fig. 7b). Point $O\left(x_o, y_o, z_o\right)$ was deemed to be a point on the separating plane. Therefore, the definition of the separating plane was given by:

$$a \cdot x + b \cdot y + c \cdot z + d = 0, \tag{3-1}$$

where, *a*, *b*, *c* and *d* were coefficients and could be calculated by the following equations:

$$\hat{N}\left(a, b, c\right) = \hat{V}_1 \times \hat{V}_2, \tag{3-2}$$

$$d = -\left(a \cdot x_o + b \cdot y_o + c \cdot z_o\right). \tag{3-3}$$

Although the separating lines were marked manually, the remaining procedures could be automatically performed by the computer. According to the separating plane, a single sweep could be divided into two parts, the valid and invalid regions. A large difference existed in reconstructed volumes between the results with and without dividing a sweep. Figure 8a gives a volume reconstructed without discarding the unnecessary speckles and the volume reconstructed using the separating plane to remove these speckles is shown in Fig. 8b. For multiple sweeps, it was necessary firstly to find out corresponding separating planes, then to conduct the same operations for removing artifacts and, finally, to combine them into a single volume according to their corresponding 3D locations in a predefined volume coordinate system. In the combination of multiple sweeps, a voxel in the region overlapped by two or more sweeps was calculated by averaging the corresponding intensities from different sweeps. If gaps resulted after the combination of the sweeps, they would not be filled in. In most cases, these gaps would be located inside the cavity of the bone. If certain gaps appeared outside of the bone and lead to an unacceptable 3D data set, the separating planes would be redefined, or the experiment would be reconducted.

Implementation and Preliminary Results

Experimental methods and the preliminary results are presented in this section. Three kinds of experiment were performed to evaluate this new scanning approach. In the first kind of experiment, we tested two phantoms to obtain quantitative results for validation and reproducibility. Firstly, a plastic tube filled with ultrasound coupling gel was used as a phantom. In order to quantify the performance of this method, two plastic

bands that were approximately parallel to each other were fastened to the body of the tube, as shown in Fig. 9a. We measured the distance between the two bands at five different positions around the tube by using a micrometer. The measured distance was 39.03±0.36 mm (mean ± SD). During scanning, the top of the tube was firmly fixed with the armrest of the auxiliary apparatus and most of the body of the tube phantom was immersed in the bag filled with water. The ultrasound probe was scanned along the external surface of the water bag. The middle part of the tube that contained the two plastic bands was scanned from the lower to the upper part and six sweeps with different probing directions were collected. We conducted four experiments on the gel tube and the corresponding four volumes were reconstructed. A typical reconstructed 3D image is shown in Fig. 9b. By using the developed functions for measurement in our program (Huang et al. 2005), the distance between the two bands was measured from the four reconstructed volume data sets, respectively. Five measurements at different part of each volume were carried out and the results are presented in Table 1. The mean distance of overall 20 measurements on the four volumes was 39.2±0.5 mm, which was very close to the results obtained by the micrometer.

In addition to the gel tube, a cylindrical silicone phantom was also used to test the accuracy and the reproducibility of this method. Similarly, the cylinder phantom was stuck to a long wooden rod that was fixed to the armrest. Four sweeps that could cover the phantom were scanned during the data acquisition for generating one volume. As only the surface of the phantom in each sweep was useful to construct the eventual volume and compute the dimensions, separating planes were defined to retain only the surface facing the probe in a B-scan. Therefore, the difference of ultrasound speed in silicone

material and water could be ignored. In this study, 10 experiments were performed and 10 volumes were reconstructed accordingly. Figure 9c shows a typical volume of the cylinder phantom. The dimensions of the phantom were measured at five different locations in each of the reconstructed volume data sets and compared with those measured by the micrometer, as presented in Table 2. The diameter and the height of the cylinder phantom were measured at five different positions using a micrometer, respectively. The volume of the cylinder phantom was calculated based on the measured diameter and height.

In the second kind of experiment, a chicken's lower leg (Fig. 10a) was fastened to a steady inflexible plastic arm and immersed in the bag filled with water. Four sweeps with different probing directions were collected and then processed using the proposed segmentation algorithm, respectively. Figure 10b shows the 3D image of reconstructed volume. A slice as shown in Fig. 10c and d was obtained from the volume data to present the interior structure of the chicken leg. The cross-sectional shape of the bone could be clearly observed. Figure 10e shows the internal anatomical structure of the chicken leg by cropping the volume data. The individual tarsometatarsus of the chicken can be identified.

The last kind of experiment was conducted on human limb extremities *in vivo*. The experimental set-up is shown in Fig. 3. The subject sat beside the auxiliary apparatus. His forearm was held by the armrest in order to keep his fingers as steady as possible during the scanning. His fingers and hand were submerged in the water bag. The ultrasound probe was moved smoothly along the external surface of the water bag. Three sweeps that covered the fingers were collected. By carefully finding the separating planes for the three sweeps, the 3D volume of the two fingers with complete anatomic structure

was obtained (Fig. 11a and b). Though errors of reconstruction existed, the fingers, including their nails, can be clearly identified. In addition, Fig. 11c and d illustrate a slice obtained from the volume to show the interior tissues of the two fingers. Figure 11e gives the internal tissues of the two fingers by cropping. The anatomic structure of the human finger can be identified in this figure. However, it could be obviously noted in Fig. 11 that the volumes reconstructed from the three sweeps did not register completely with each other. This artifact was mainly caused by the movement of the hand during the scanning of different sweeps, though the armrest was used to make the hand as steady as possible during the scanning. This problem is expected to be solved either by designing better methods or tools to keep the subject's limbs more stable, or by applying algorithms for registration of adjacent B-scans and that of multiple sweeps. Several algorithms reported by Treece et al. (2002) and Gee et al. (2003b) would be helpful for the solutions of registration in this study. Also, system errors had inevitably contributed to the inaccurate reconstruction. This issue will be further discussed in the next section.

Discussion

In comparison with previous mechanical methods (Douglas et al. 2002), freehand 3D ultrasound can offer complete freedom to guide the ultrasound probe along the path of anatomy (Treece et al. 2003). The preliminary results demonstrated that the new freehand scanning approach adopted in this study using a water bag is feasible to collect 2D images around limb extremities for constructing 3D volumes with their complete anatomic structure. In addition, as the ultrasound probe only contacted with the external surface of the water bag during the scanning process, the deformation of tissues caused

by directly a contact between the probe and the surface of body parts was avoided. Moreover, this new approach could be used to scan body parts with relatively complex contours, such as hands and feet.

Despite the successful implementation of this proposed scanning method, the reconstructed volume of human fingers still contained errors, as shown in Fig. 11. A number of error sources could lead to the distortion of the reconstructed 3D volume (Treece et al 2003). The errors caused by calibration, artifacts in B-mode images and the movement of body tissues were discussed as follow.

The movement of the body parts during the scanning might be the main source of the anatomy distortion in this study. As described earlier, an auxiliary apparatus was designed to fix the water bag and support the subject's limb extremities by an armrest. However, it was difficult for the subjects to maintain their limbs without any motion during the three sweeps, which lasted for approximately 1 min. To solve this problem, registration algorithms within single sweep and between sweeps have to be implemented. Treece et al. (2002) and Gee et al. (2003b) proposed algorithms for the registration in freehand 3D ultrasound imaging when the tissue was compressed by the probe and presented good results. However, their algorithms cannot be directly used for the registration required in this study, as their artifacts caused by probe compression could be successfully avoided using a water bag. Further efforts should be made to investigate efficient registration algorithms to compensate for the movement of the body parts during the scanning process so as to construct volumes with more accurate 3D anatomic structure.

The calibration (spatial calibration and temporal calibration) errors could be another cause of mismatch of the sweeps (Fig. 11). Even though good calibrations could be achieved for the electromagnetic spatial sensing device (Prager et al. 1998), registration of multiple sweeps was necessary (Gee et al. 2003b). The artifacts in B-mode images included noise caused by bubbles in water and the strong attenuation of ultrasound signal by bones, as described earlier. Although a semiautomatic algorithm was used to remove most of the unnecessary speckles behind the bone, many artifacts caused by these speckles still existed in B-mode images. Furthermore, the segmentation result greatly depends on the operator's experience when using this semiautomatic method. According to our experiments, some useful anatomical information might not be well preserved within all sweeps if the separating lines were not properly defined. Therefore, gaps would result in the combined volume (Fig. 10d). For the experiments of human fingers *in vivo*, as the fingers contacted with each other during the scanning, the soft tissues near the contacting interface could only be scanned by the front and back sweeps; hence, some information tended to be left out if the two valid regions defined by the separating lines for the two sweeps were not overlapped. How fully to remove artifacts and keep the original information of anatomy remains a challenge in the field of ultrasound image processing. Therefore, one of our future research tasks will be focused on the development of fully automatic segmentation algorithm for removing artifacts in ultrasound images during the volume reconstruction of musculoskeletal body parts.

In summary, a new scanning approach using a water bag was proposed to acquire ultrasound images of limb extremities from various directions. The acquired B-mode images contained complete anatomic information of limb parts and were used to

construct 3D volume. A new semiautomatic segmentation algorithm was also proposed for removing artifacts in B-mode images. Preliminary results obtained for phantoms, animal tissues *in vitro* and human tissues *in vivo* demonstrated the feasibility of these new approaches. The movement of the body parts inside the water bag during the scanning needs to be solved before the potential of this new scanning approach can be fully realized.

Acknowledgements

This work was partially supported by the Research Grants Council of Hong Kong (PolyU 5245/03E).

References

Douglas T, Solomonidis S, Sandham W, Spence W**.** Ultrasound imaging in lower limb prosthetics. IEEE Trans Neur Sys Reh 2002; 10: 11-21.

Gee AH, Prager RW, Treece GM, Berman L. Engineering a freehand 3D ultrasound system. Pattern Recog Lett 2003a; 24: 757-777.

Gee AH, Treece GM, Prager RW, Cash CJC, Berman L. Rapid registration for wide field of view freehand three-dimensional ultrasound. IEEE Trans Med Imaging 2003b; 22: 1344-1357.

He P, Xue KF, Chen Q, Murka P, Schall S. A PC-based ultrasonic data acquisition system for computer-aided prosthetic socket design. IEEE Trans Rehab Eng 1996; 4: 114–119.

Huang QH, Zheng YP, Lu MH, Chi ZR. Development of a portable 3D ultrasound imaging system for musculoskeletal tissues. Ultrasonics 2005; 43: 153-163.

Lieber RL, Friden J. Functional and clinical significance of skeletal muscle architecture. Muscle Never 2000; 23: 1647-1666.

Martinoli C, Bianchi S, Dahmane M, Pugliese F, Bianchi-Zamorani MP, Valle M. Ultrasound of tendons and nerves. Eur Radiol 2002; 12: 44-55.

Nelson TR, Pretorius DH. Three-dimensional ultrasound imaging. Ultrasound Med Biol 1998; 24: 1243-1270.

Prager RW, Rohling RN, Gee AH, Berman L. Rapid calibration of 3-D freehand ultrasound. Ultrasound Med Biol 1998; 24: 855-869.

Treece GM, Gee AH, Prager RW, Cash CJC, Berman LH. High-definition freehand 3-D ultrasound. Ultrasound Med Biol 2003; 29: 529-546.

Treece GM, Prager RW, Gee AH, Berman L. Correction of probe pressure artifacts in freehand 3D ultrasound. Med image Anal 2002; 6: 199-214

Winter TC, Teefey SA, Middleton WD. Musculoskeletal ultrasound: an update. Radiol Clin North Am 2001; 39: 465-483.

Figure captions

Fig. 1. The diagram of typical freehand 3D ultrasound imaging system using electromagnetic spatial sensor.

Fig. 2. A typical 2D ultrasound image containing musculoskeletal tissues and artifacts.

Fig. 3. The experimental set-up using an auxiliary apparatus.

Fig. 4. The scanning protocol using a bag filled with water.

Fig. 5. Multiple sweeps used for constructing volumes in full shape. (a) The image stacks of three sweeps with different probing directions and moving directions; (b) A schematic showing how cover the entire limb extremity; and (c) A combined image stack of the three sweeps in the 3D space.

Fig. 6. A plane for separating the valid region and invalid region within a single sweep. The valid region mainly contains those soft tissues above the bones and is retained, while the invalid region mainly contains unnecessary speckles below the bones and is removed before volume reconstruction.

Fig. 7. Illustrations showing how a separating plane for segmentation is defined. (a) Two separating lines are manually marked within a single sweep; and (b) The separating plane can be identified based on the four points (*A*, *B*, *C*, *D*) using eqns (1), (2) and (3).

Fig. 8. Typical volumes of the fingers reconstructed from a single sweep. (a) The volume reconstructed without using a separating plane; and (b) The volume reconstructed using a separating plane.

Fig. 9. Results of the plastic tube filled with ultrasound gel. (a) The real image of the tube with the two plastic bands, between which the distance is indicated by an arrow; (b) The reconstructed 3D image of the middle part of the tube with an arrow indicating the measured distance; and (c) The reconstructed 3D image of the cylinder phantom.

Fig. 10. Results of a chicken leg scanned *in vitro*. (a) The real image of the chicken leg; (b) the reconstructed volume using the water bag; (c) (d) Showing that a slice is obtained from the volume; and (e) Showing the cropped 3D volume that presents the internal anatomical structure of the chicken leg.

Fig. 11. A volume reconstructed from two human fingers *in vivo*. (a) The front view of the two fingers; (b) The back view of the two fingers; (c) (d) Showing that a slice is obtained from the volume; and (e) Showing the cropped 3D volume that gives the internal anatomical structure of the two fingers.

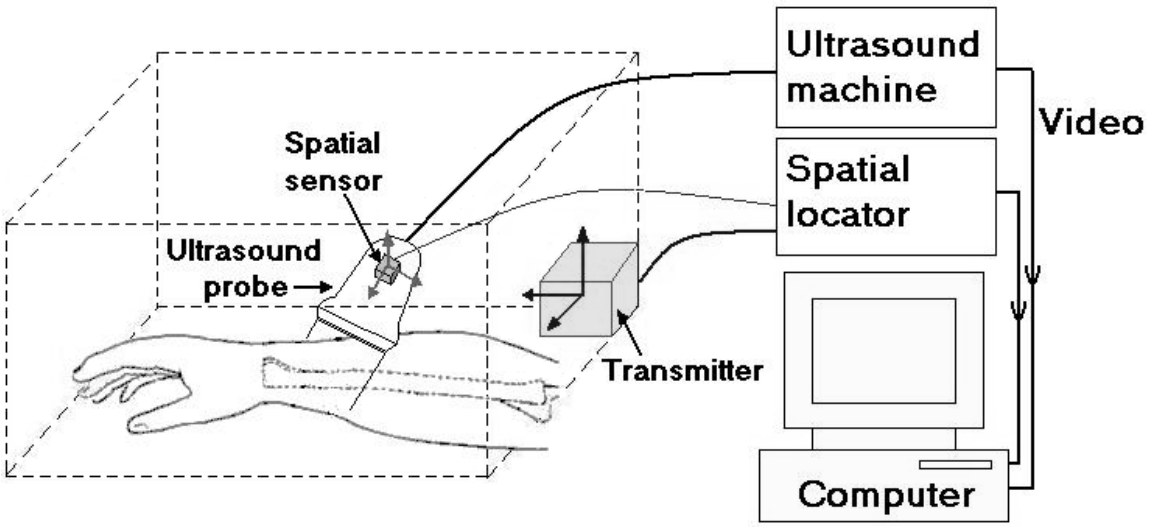
Ultrasound machine
Video
Spatial sensor
Spatial locator
Ultrasound probe
Transmitter
Computer

Fig. 1

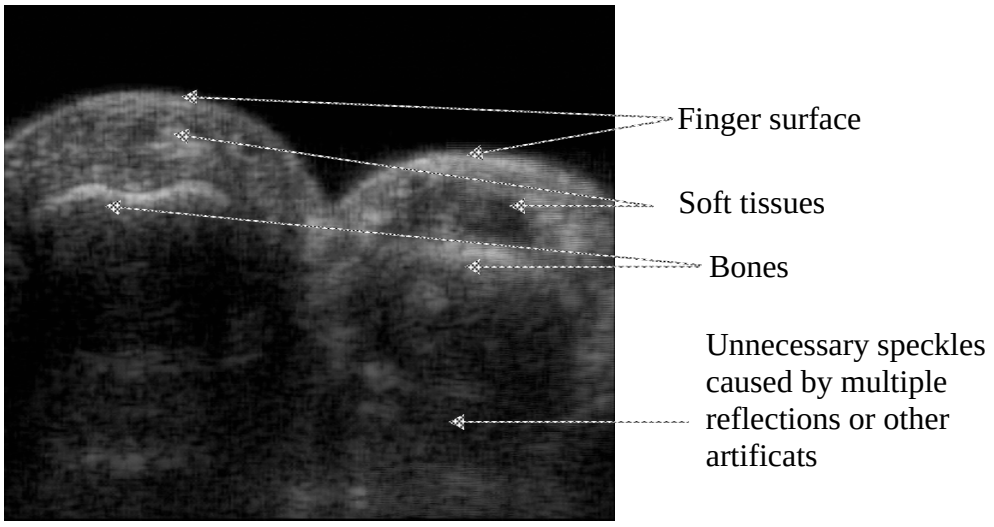
Finger surface
Soft tissues
Bones
Unnecessary speckles caused by multiple reflections or other artificats

Fig. 2

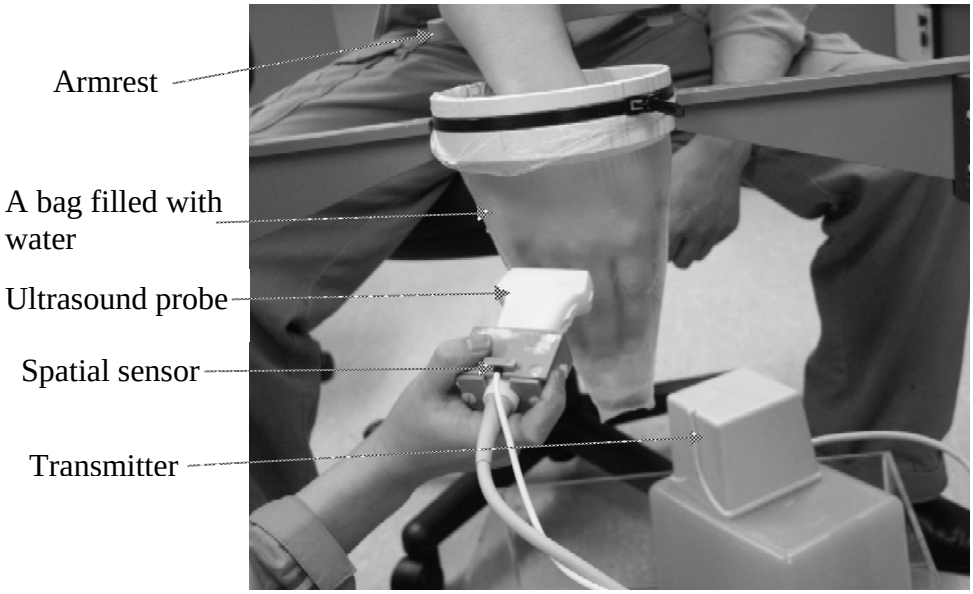
Armrest
A bag filled with water
Ultrasound probe
Spatial sensor
Transmitter

Fig. 3

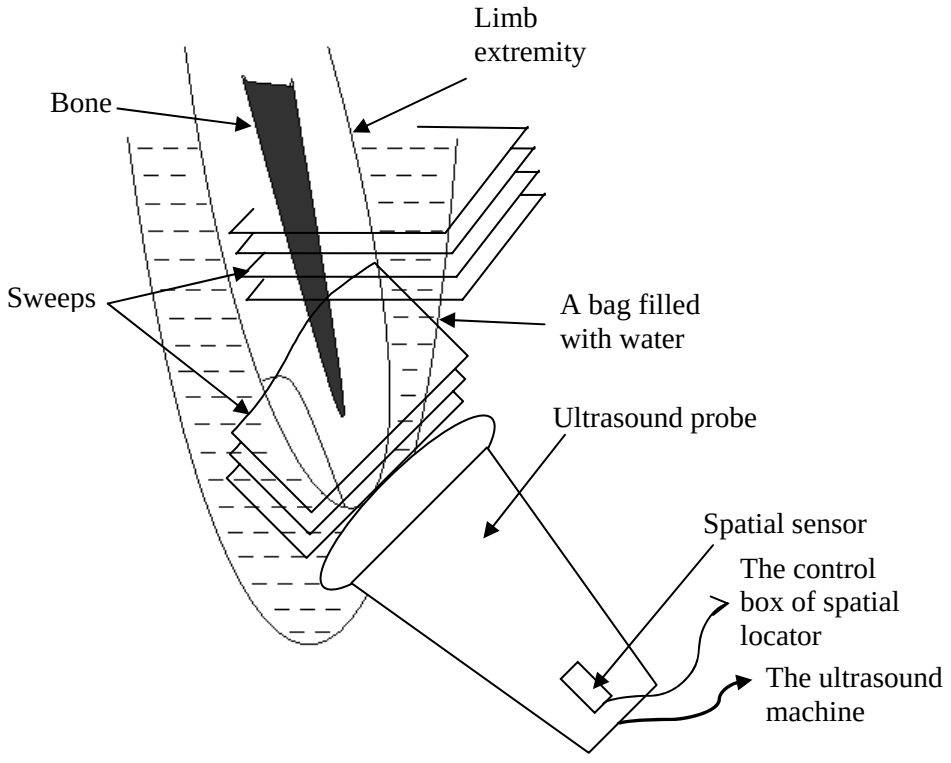
Limb extremity
Bone
Sweeps
A bag filled with water
Ultrasound probe
Spatial sensor
The control box of spatial locator
The ultrasound machine

Fig. 4

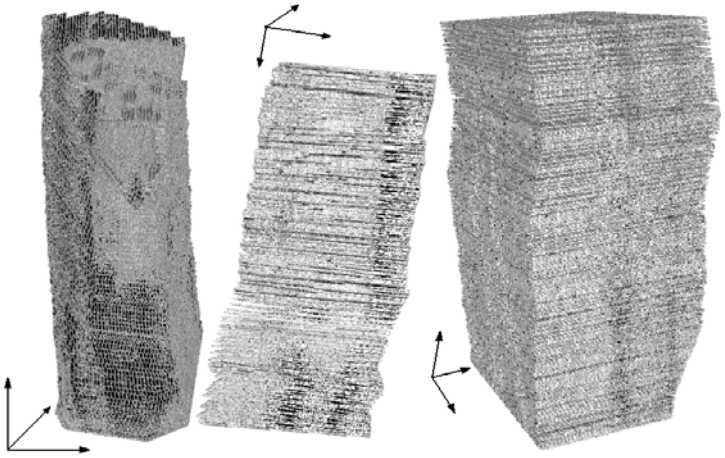

Fig. 5(a)

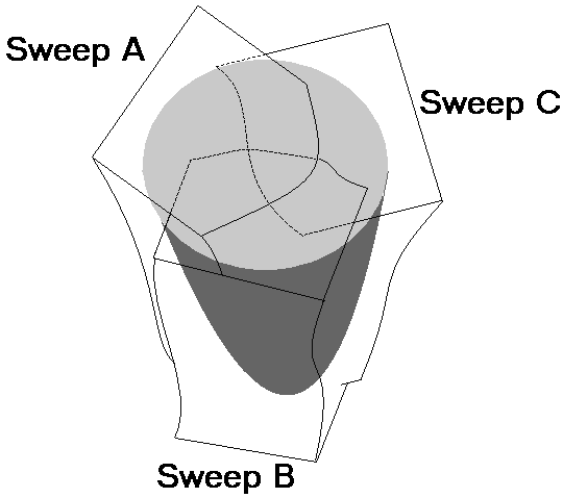

Fig. 5(b)

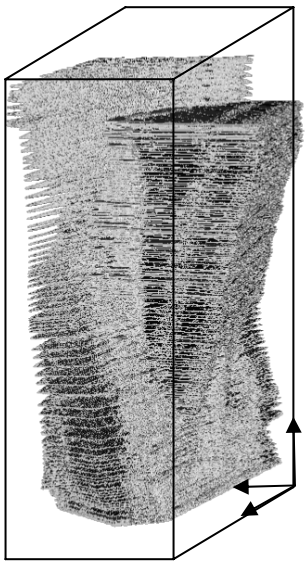

Fig. 5(c)

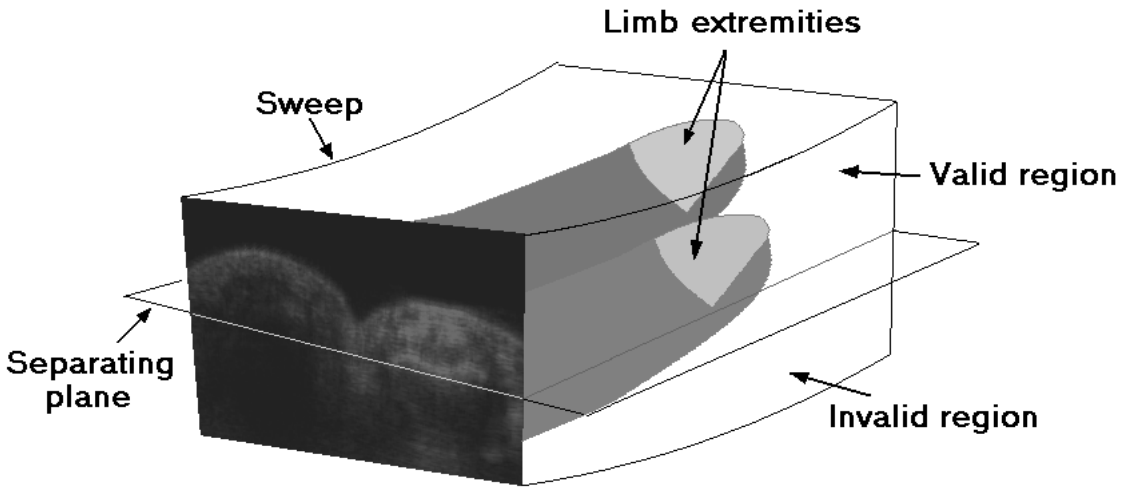

Fig. 6

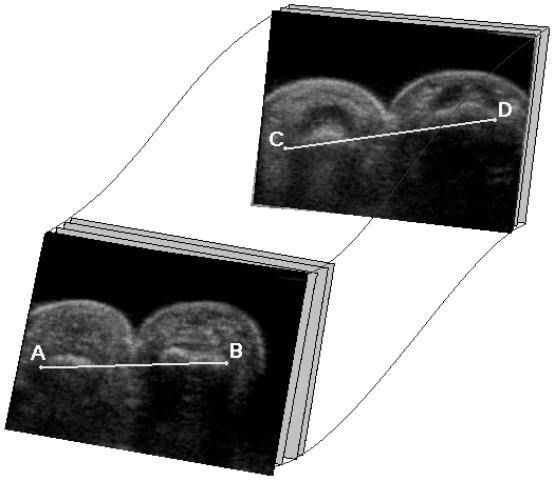

Fig. 7(a)

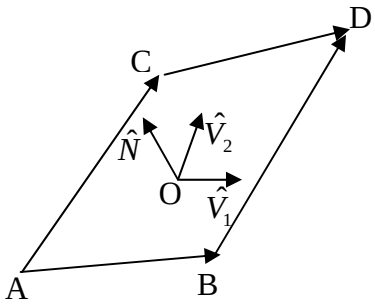

Fig. 7(b)

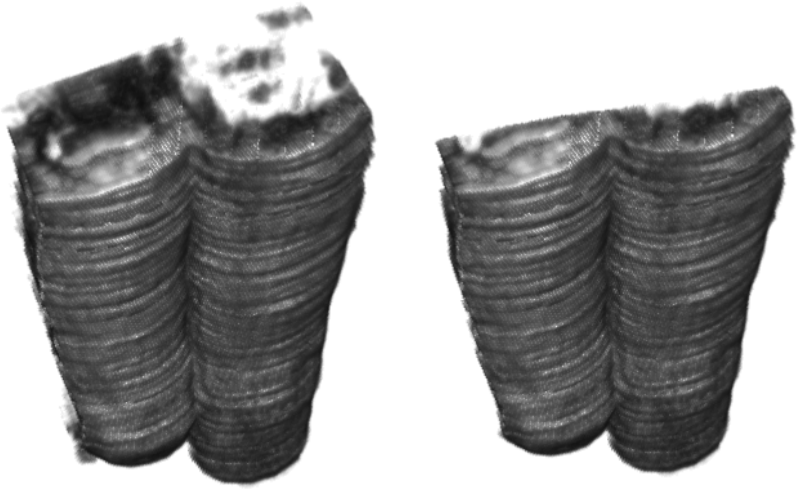

Fig. 8(a) Fig. 8(b)

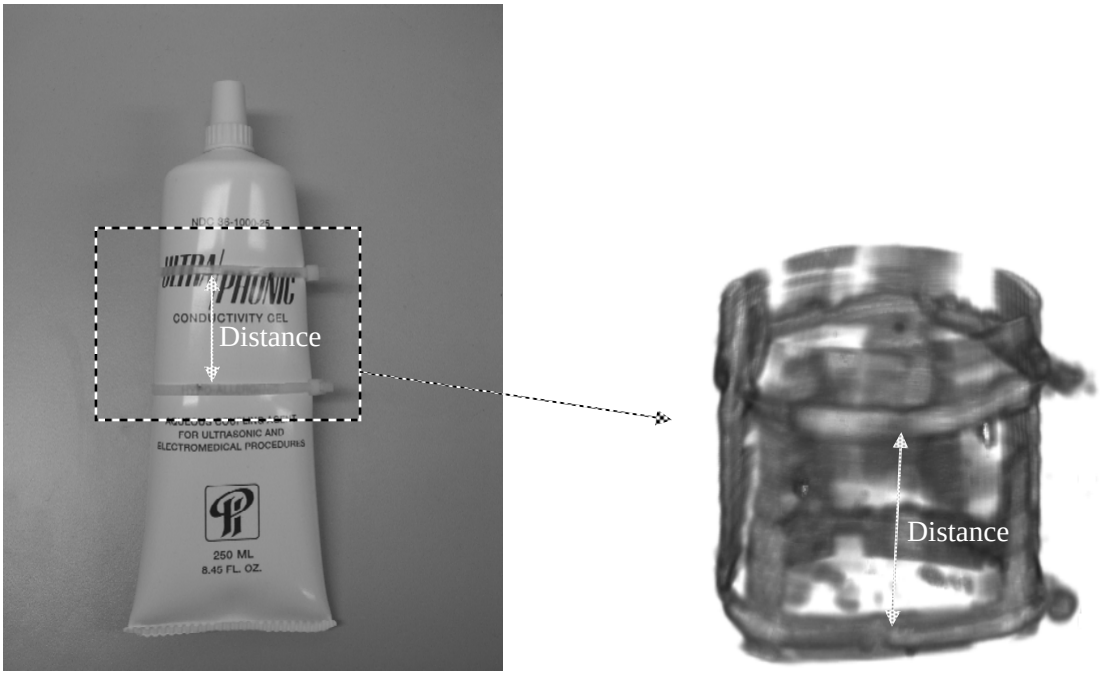

Fig. 9(a) Fig. 9(b)

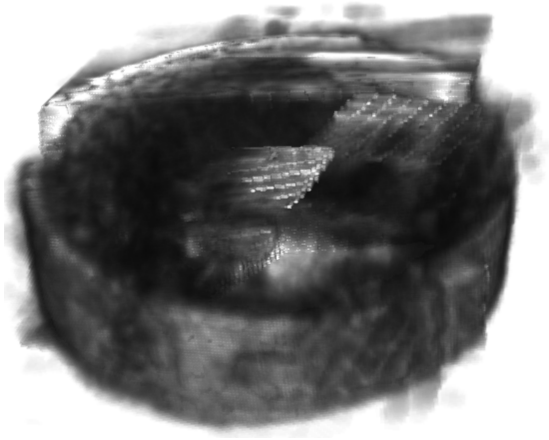

Fig. 9(c)

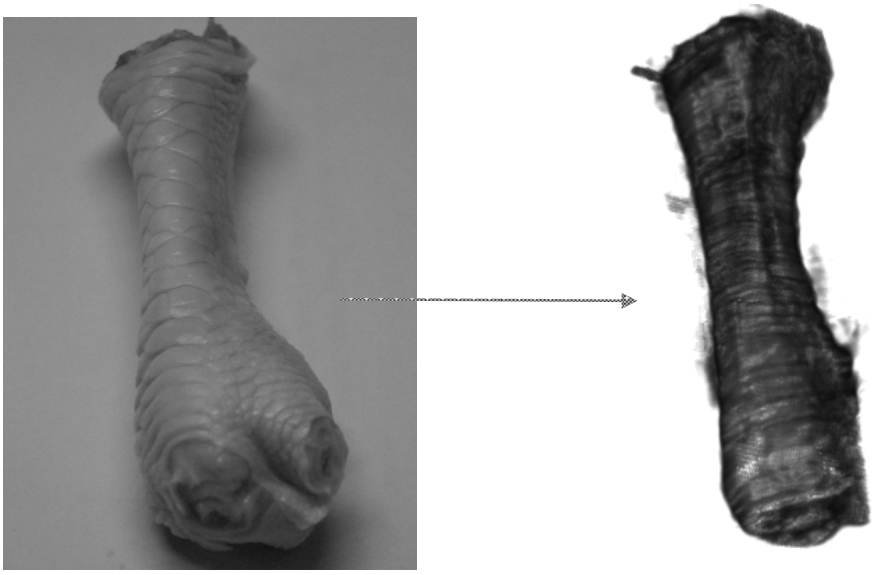

Fig. 10(a) Fig. 10(b)

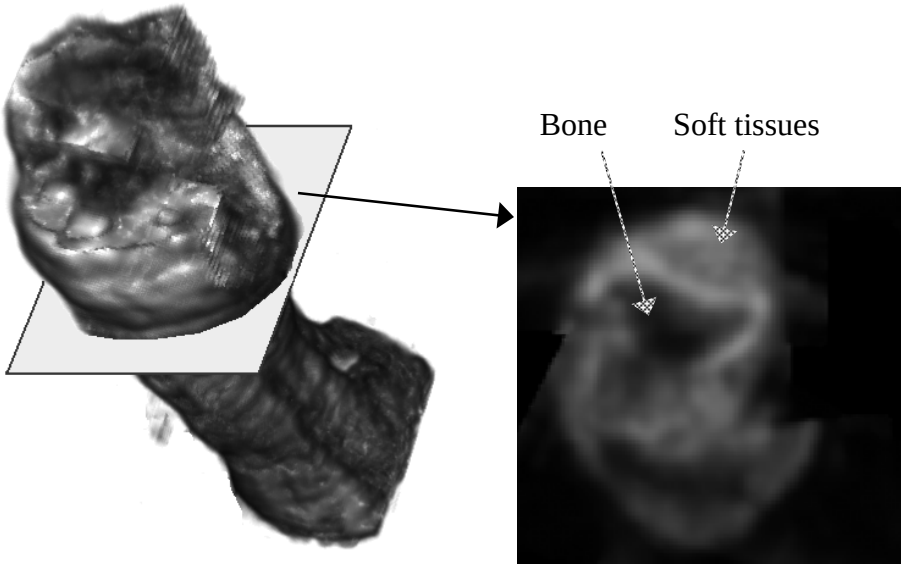

Fig. 10(c) Fig. 10(d)

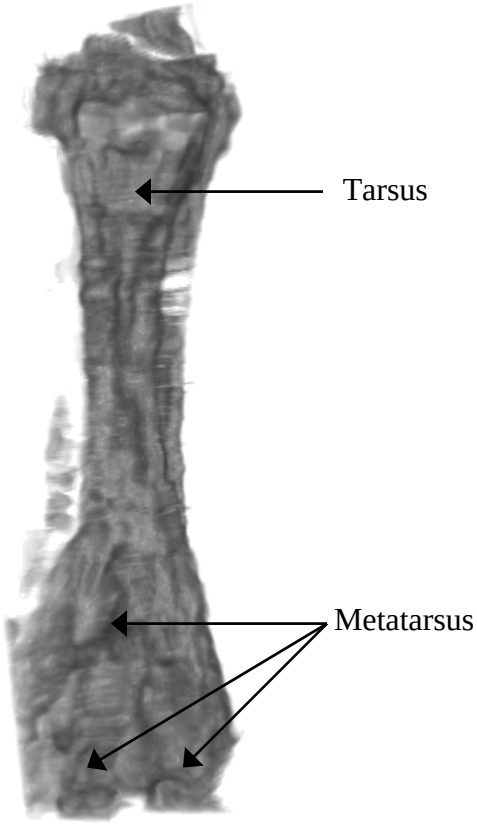

Fig. 10(e)

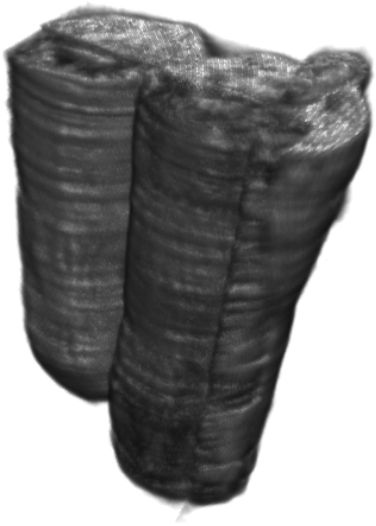

Fig. 11(a)

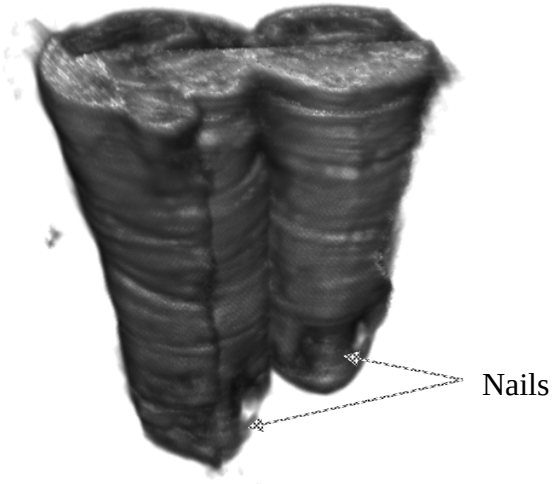

Fig. 11(b)

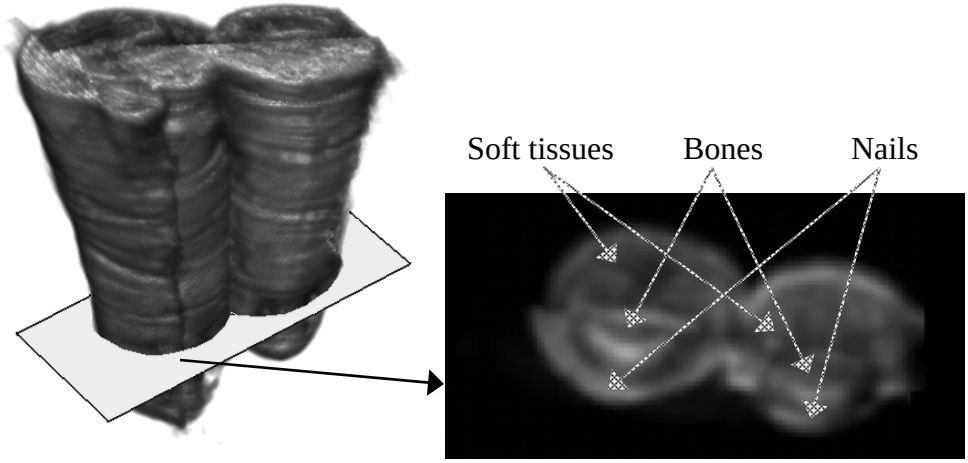

Fig. 11(c)

Fig. 11 (d)

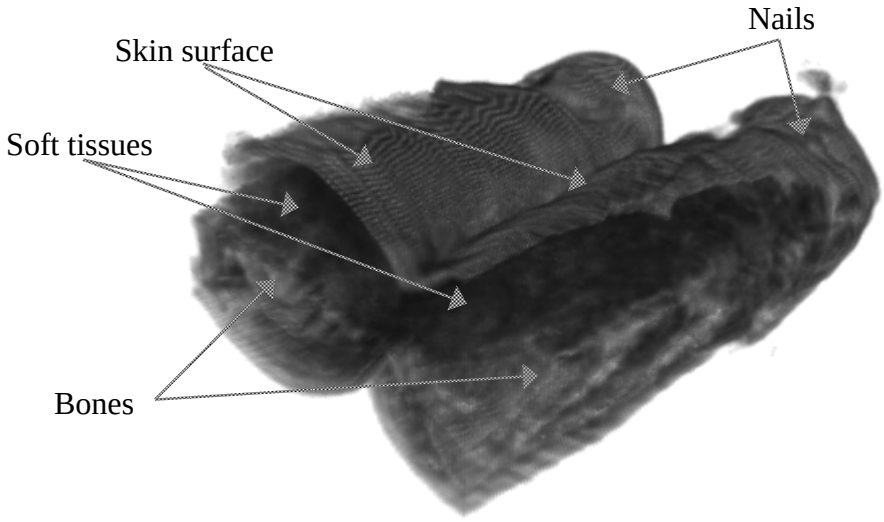

Fig. 11 (e)

Tables

Table 1. Quantitative comparison of the measurement of the distance between the two bands surrounding on the gel tube.

Table 2. Quantitative measurements of the cylinder phantom using the volume data in comparison with the results measured by the micrometer. The results were averaged from the 10 sets of measurement.

Table 1.

Distances (mm) measured using volume data (mean±SD)		Distance (mm) measured with micrometer (mean±SD)
Volume 1	39.3±0.4	39.03±0.36
Volume 2	39.0±0.5	
Volume 3	39.2±0.7	
Volume 4	39.1±0.6	

Table 2.

Measurement on 3D volumes (mean±SD)		Measurement by micrometer (mean±SD)
Diameter (mm)	40.2±1.4	41.29±0.13
Height (mm)	12.9±1.0	12.98±0.17
Volume (mm^3)	16400±1600	17370±140